PHYSICAL REVIEW B VOLUME 45, NUMBER 8 15 FEBRUARY 1992-II

Dynamics of induced absorption and gain related to excitonic excitation in CuCl

R. Leonelli,* A. Manar,† J. B. Grun, and B. Hönerlage
Institut de Physique et Chimie des Matériaux de Strasbourg, Groupe d'Optique Nonlinéaire et d'Optoélectronique,
5 rue de l'Université, 67084 Strasbourg CEDEX, France

(Received 29 July 1991)

We present a thorough investigation of the different relaxation channels opened in a strongly interacting system of excitonic quasiparticles in CuCl for density regimes ranging up to 50 MW/cm^2. A spectrally narrow pump beam consisting of 30-ps pulses is tuned around one-half the biexciton energy. It creates an initial distribution of biexcitons through resonant two-photon absorption. A spectrally broad probe beam made of pulses that also have 30-ps duration monitors the excitation-induced variation of the transmission spectrum of CuCl samples near the Z_3 exciton resonance. Coherent processes corresponding to parametric emissions of various orders are observed. Absorption and gain bands that reflect the evolution of biexciton and exciton populations on their respective dispersion curves are followed as functions of the time delay between pump and probe pulses.

I. INTRODUCTION

The optical properties close to the absorption edge of semiconductors with large, direct band gaps are governed by excitonic resonances. If excitonic transitions are dipole allowed, the corresponding exciton states are strongly coupled to the electromagnetic light fields. The propagating modes in the crystal are mixed states of both fields. The resulting quasiparticles are called excitonic polaritons.[1-3] Density-dependent interactions of polaritons with other quasiparticles result in nonlinear-optical effects which give rise to absorption changes and anomalies in their dispersion.[4,5] These nonlinear effects have attracted much interest because of their importance in the understanding of the fundamental properties of semiconductors and of their potential applications for optoelectronic devices.

Copper chloride is a particularly interesting system because of its simple band structure and large exciton binding energy (190 meV). The lowest-lying excitonic resonance, which comes from the Γ_5-symmetry part of the Z_3 exciton series, is optically active and spectrally well separated from other resonances. Moreover, excitons can couple to form excitonic molecules or biexcitons that also have a large binding energy (32 meV). In CuCl, these biexcitons cannot be directly created by one-photon transitions. They can, however, be directly generated by simultaneous two-photon absorption (TPA) from the crystal ground state, or from populated excitonic states by an induced one-photon absorption. A huge oscillator strength is associated with these transitions, mostly because of the spatial extent of the biexciton wave function. An additional resonance enhancement in TPA is due to the proximity of the dipole-active exciton states.[6] Near the Z_3 exciton resonance, CuCl can thus be described as a three-level system[7]: the crystal ground state $|1\rangle$, the transverse exciton state $|2\rangle$, and the biexciton state $|3\rangle$ [Fig. 1].

The properties of these states have been intensively investigated through nonlinear spectroscopy, but most measurements were performed at low excitation intensities in order to avoid intensity-induced changes. For example, hyper-Raman scattering[4,8-11] and two-photon absorption spectroscopy[4,12,13] have been used to study the Z_3 exciton and the associated polariton structures. The characteristics of the biexciton ground state (energy at the center of the Brillouin zone, symmetry, dispersion in momentum space) have been obtained by the study of resonant two-photon absorption.[14-17] Picosecond time-resolved spectroscopy of the absorption induced by a light excitation above the band gap,[18] and in the upper branch of the polaritons,[19] has led to an understanding of some of the exciton and biexciton relaxation processes.

Under high light-excitation conditions, anomalies appear in the complex dielectric function. Under quasistationary excitation conditions, these effects have been theoretically investigated using a Green's-function approach[20,21] and a density-matrix formalism.[22-24] The real part of the complex dielectric function, which gives the density dependence of the polariton dispersion, has been experimentally studied by hyper-Raman scattering and nondegenerate four-wave mixing.[4,6,,25-27] These nonlinear characteristics have been shown to result in optical bistability[28,29] and optical phase conjugation.

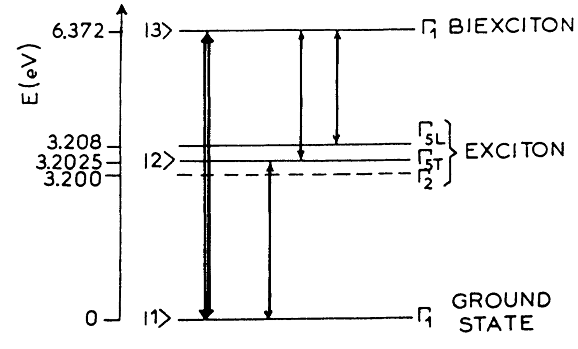

FIG. 1. The different exciton and biexciton energy levels and the allowed one-photon transitions (single arrows) and two-photon transitions (double arrows).

In the high-density and short-time regime, the dynamical relaxation process of the exciton and biexciton populations shows up in the nonlinear effects. Therefore, they can be studied spectroscopically, especially by means of picosecond time-resolved transmission spectroscopy. We present in this publication such pump and probe transmission measurements performed with a time resolution of 20 ps.

II. THEORETICAL DESCRIPTION OF TRANSIENT OPTICAL NONLINEARITIES IN CuCl

As already stated, CuCl is well described by a three-level system. One-photon transitions are allowed between exciton and biexciton states. In addition, two-photon transitions are allowed between the crystal ground state and the biexciton state if the two photons have parallel polarizations. This system gives rise to strong optical nonlinearities, especially when the driving light field is tuned into the two-photon resonance. These nonlinearities are best described through the formalism developed in Ref. 30 which uses the full nonlinear dielectric function. In particular, this formalism allows a separation of the nonlinear susceptibility into coherent and incoherent parts. The coherent parts are driven by the pump beam and are important for pulse-propagation and signal-generation processes. Their time dependence reflects the coherence time of the driving light field and that of the generated quasiparticles. The latter one is usually dependent on the density of all the existing quasiparticles. The incoherent parts arise since coherently created biexcitons relax through collision processes and populate other states which have no definite phase relation with the driving light field. Thus, an incoherent exciton and biexciton population is generated. As we have stated above, this exciton population gives rise to an induced absorption while that of the biexciton gives rise to gain. Both lead to induced refractive index changes. Their time-dependent spectral behavior gives information on the energy distribution, on the coherence time, and on the lifetime of the quasiparticles.

Let us consider a pump beam and a test beam interacting in a nonlinear medium. Parametric processes involving these two coherent optical fields will generate a signal beam which has to be considered in the linear wave equation. Following Ref. 31, we write for the optical fields,

$$E_i(z,t)=\tfrac{1}{2}[E_i^0(z,t)e^{i(\omega_i t-k_i z)}+\text{c.c.}]\ , \tag{1}$$

where the index i refers to the pump, test, or signal beams respectively. The wave equation then reads

$$\frac{\partial^2}{\partial z^2}E_i(z,t)-\mu_0\sigma\frac{\partial}{\partial t}E_i(z,t)-\mu_0\epsilon_L\frac{\partial^2}{\partial t^2}E_i(z,t)=\mu_0\frac{\partial^2}{\partial t^2}P_{\text{NL}}^i(z,t)\ . \tag{2}$$

Here, σ is the conductivity, μ_0 the permeability, and $\epsilon_L=\epsilon_0(1+\chi_L)$ the linear dielectric function of the medium. $P_{\text{NL}}^i(z,t)$ is the nonlinear polarization associated with the ith beam. We assume a local spatial response,

$$P_{\text{NL}}^i(z,t)=\sum_j\int_{-\infty}^{t}\chi_{\text{NL}}^{ij}(z,t,t')E_j(z,t')dt'\ , \tag{3}$$

where χ_{NL}^{ij} is the nonlinear susceptibility tensor. It can be separated into rapidly and slowly varying parts:[30]

$$\chi_{\text{NL}}^{ij}(z,t,t')=\sum_{n,n'}\chi_{\text{NL}}^{ij(n,n')}(z,t,t')\times e^{in(\omega t-kz)}e^{in'(\omega_j t-k_j z)}\ . \tag{4}$$

In the case of coherent processes, ω and $\mathbf{k}$ are equal to the frequency and wave vector of the pump beam. If incoherent processes are involved, ω and $\mathbf{k}$ rather describe the frequency and wave vector of the excited quasiparticles. If the field amplitudes $E_i^0(z,t)$ vary slowly in time with respect to $\chi_{\text{NL}}^{ij(n,n')}$, we may define frequency-dependent susceptibility components by

$$\chi_{\text{NL}}^{ij(n,n')}(z,t,\omega)=\int_0^\infty\chi_{\text{NL}}^{ij(n,n')}(z,t,t')e^{-i\omega t'}dt'\ . \tag{5}$$

Using Eqs. (1), (3), and (5), we now obtain

$$P_{\text{NL}}^i(z,t)=\tfrac{1}{2}\left[\sum_{j,n,n'}\chi_{\text{NL}}^{ij(n,n')}(z,t,\omega_j)E_j^0(z,t)\exp\{i[n\omega+(n'+1)\omega_j]t-i[nk+(n'+1)k_j]z\}\right.$$
$$\left.+\sum_{j,n,n'}\chi_{\text{NL}}^{ij(-n,-n')*}(z,t,\omega_j)E_j^{0*}(z,t)\exp\{i[n\omega+(n'-1)\omega_j]t-i[nk+(n'-1)k_j]z\}\right]\ . \tag{6}$$

Within the slowly varying envelope approximation, all time derivatives of E_j^0 and $\chi_{\text{NL}}^{ij(n,n')}$ can be assumed to be small compared to $\omega_j E_j$ and $\omega\chi_{\text{NL}}^{ij(n,n')}$. Similarly, $\partial^2E_j^0/\partial z^2\ll k_j\partial E_j^0/\partial z$. Moreover, ω_j and k_j satisfy the dispersion relation

$$\mu_0\epsilon_L\omega_j^2=k_j^2\ . \tag{7}$$

$$-2ik_i\frac{\partial}{\partial t}E_i^0-i\omega_i\mu_0\sigma E_i^0=-\mu_0\left[\sum_{n,n',j}[n\omega+(n'+1)\omega_j]^2\chi_{\rm NL}^{ij(n,n')}(z,t,\omega_j)E_j^0(z,t)\right.$$
$$\times\delta(n\omega+(n'+1)\omega_j-\omega_i)\delta(nk+(n'+1)k_j-k_i)$$
$$+\sum_{n,n',j}[n\omega+(n'-1)\omega_j]^2\chi_{\rm NL}^{ij(-n,-n')*}(z,t,\omega_j)E_j^{0*}(z,t)$$
$$\left.\times\delta(n\omega+(n'-1)\omega_j-\omega_i)\delta(nk+(n'-1)k_j-k_i)\right]\,. \tag{8}$$

Finally, we can assume the test and signal beams to be weak enough so that they do not affect $\chi_{\rm NL}^{ij}$. The test field then obeys

$$\frac{\partial}{\partial z}E_t^0(z,t)=-\frac{\omega_t\mu_0\sigma}{2k_t}E_t^0(z,t)+\chi_{\rm NL}^{tt(0,0)}(z,t,\omega_t)\frac{\mu_0\omega_t^2}{2ik_t}E_t^0(z,t)$$
$$+\chi_{\rm NL}^{ts(-2,0)*}(z,t,\omega_s)\frac{\mu_0(2\omega_p-\omega_s)^2}{2ik_t}E_s^{0*}(z,t)\delta(2\omega_p-\omega-\omega_s)\delta(2k_p-k_t-k_s)\,. \tag{9}$$

The first term on the right corresponds to the linear absorption. The second term describes the nonlinear absorption, proportional to $\mathrm{Im}[\chi_{\rm NL}^{tt(0,0)}(\omega_t)]$ and the dispersion changes, proportional to $\mathrm{Re}[\chi_{\rm NL}^{tt(0,0)}(\omega_t)]$. $\chi_{\rm NL}^{tt(0,0)}$ does not depend on whether the excited biexciton or exciton populations created by the pump beam are still coherent or not. The last term, which involves $\chi_{\rm NL}^{ts(-2,0)*}$, represents the coherent generation of a signal beam at $\omega_s=2\omega_p-\omega_t$.

III. EXPERIMENTAL PROCEDURE

The samples studied are CuCl platelets (thickness of about 30 μm) grown by vapor-phase transport. They are mounted strain free and cooled down to 4.2 K in a continuous helium-flow cryostat.

The experimental arrangement is shown in Fig. 2. A Nd^{3+}: YAG (yttrium aluminum garnet) oscillator, mode locked by a saturable absorber and an acousto-optic modulator, delivers a train of 11 infrared pulses at 1064 nm of 30 ps duration each with a repetition rate of 10 Hz. The oscillator output is sent into two different amplification paths. In the first one, the whole train is amplified and fed successively into two nonlinear crystals (*KD***P*). The third harmonic (354 mm) of the amplified infrared beam has an energy of 4 mJ per pulse train. It serves to synchronously pump a dye laser with BiBuQ 4,4‴-Bis-(2-butyloctyloxy)-*p*-quarterphenyl in toluene as the active medium. This laser is tunable in the spectral range from 375 to 400 nm (3.1 – 3.3 eV) by means of a grating working in a Littrow configuration. In the second path, the central pulse of the oscillator train is selected by a Pockels cell, amplified and frequency tripled. A single ultraviolet pulse of 30 ps duration and of 1 mJ is thus generated. This pulse is sent into two different optical-delay lines and focused into two cells containing BiBuQ in toluene. The first one generates the pump beam at a photon energy $\hbar\omega_p$ by selectively amplifying the second (most intense) pulse of the tunable laser output train by a factor of about 100. The super-radiant emission of the second one serves as the test beam. It has a spectral bandwidth of 80 meV centered at 3.2 eV. The duration of both pump and test pulses were measured on an ARP (Applications de la Recherche en Photonique) streak camera and found to be 30±5 ps. For the purpose of the experiments presented here, the pump beam was tuned to a photon energy $\hbar\omega_p=3.1860\pm0.0001$ eV. It is sent into a stepping-motor-controlled variable optical-delay line, attenuated by polarization filters and finally focused into a 150 μm spot impinging on the sample under an angle of 12±1°. The power density on the crystal could be varied in the 1.5- to 50-MW cm^{-2} range. The test beam is focused into a 80-μm spot inside the spot of the pump beam. It is normally incident on the surface of the samples. The

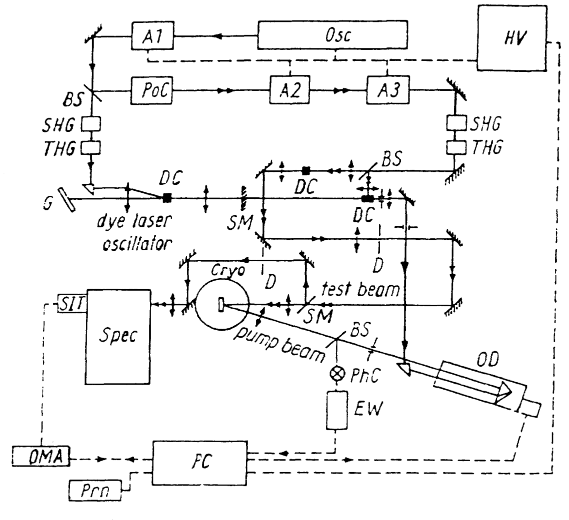

FIG. 2. The experimental setup. Osc, Nd:YAG laser oscillator; A1–A3, three Nd:YAG amplifiers; HV, high-voltage generator for flash lamps; PoC, Pockels cell; SHG and THG, second and third harmonic generators; G, Grating; DC, dye cells, OD, optical-delay line with stepper-motor drive; Cryo, liquid-helium flow cryostat; Spec, Spectrograph; HPC, 16-bit microcomputer; Prn, graphic printer; PhC, photoelectric cell; EW, energy-window discriminator. Solid lines, optical paths; dotted lines, electrical wirings.

transmitted test beam is sent through an iris diaphragm to eliminate spurious luminescence and pump laser-diffused light. It is then focused onto the entrance slit of a Huet spectrograph (focal length 65 cm, resolution 0.2 meV) and detected by a PAR (Princeton Applied Research) optical multichannel analyzer. The time delay τ between pump and test pulses as a function of the variable delay line position was independently checked by inserting an optical Kerr shutter activated by a pulse from a third beam (the 1064-nm output of the second amplification path) between the sample and the entrance slit of the spectrograph. The intensity of each pump pulse is monitored. Accumulation by the data acquisition system is allowed only if this intensity falls within an acceptable range ($\pm 10\%$ of an average value).

Care is taken to ensure that the changes observed in the transmitted test beam in the presence of the pump beam come from induced absorption processes. The small luminescence signal still collected at higher pump intensities is subtracted from the data. The reflected test beam intensity is also monitored. It is observed that even at the highest pump-power density, the reflectivity of the samples in the spectral region studied is not altered.

IV. EXPERIMENTAL RESULTS

The energy levels of excitons and biexcitons in CuCl are schematically drawn in Fig. 1. Their symmetries at the center of the Brillouin zone are indicated. The allowed one- and two-photon transitions are represented by arrows in Fig. 1. The exciton-polariton dispersion is drawn in Fig. 3 as solid lines. They are determined by the following (linear) relations, as given by Hopfield:[1]

$$\frac{Q^2c^2}{\omega^2}=\epsilon_b\left[\frac{E_L(Q)^2-\hbar^2\omega^2}{E_T(Q)^2-\hbar\omega^2}\right], \tag{10}$$

where Q is the wave vector of the exciton polariton, $\hbar\omega$ is the photon energy, and c the light velocity,

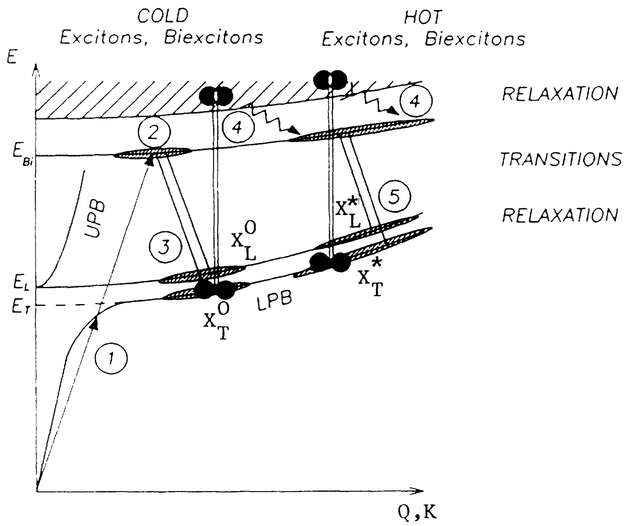

FIG. 3. Exciton polariton and biexciton-dispersion curves for CuCl and schematic representation of principal exciton and biexciton processes [(1)–(5)].

$$E_T(Q)=E_T+\frac{\hbar^2Q^2}{2m_{\rm ex}}, \tag{11}$$

$$E_L(Q)=E_L+\frac{\hbar^2Q^2}{2m_{\rm ex}}, \tag{12}$$

where E_T (E_L) is the transverse (longitudinal) exciton energy, $m_{\rm ex}$ is the mass governing the exciton center of mass motion, and ϵ_b is the background dielectric constant.

These parameters are well known from spectroscopic measurements,[10]

$$E_T=3.2025\text{ eV}, \quad E_L=3.208\text{ eV}, \quad m_{\rm ex}=2.5m_0, \quad \epsilon_b=5 \tag{13}$$

(m_0 is the free-electron mass).

The dispersion relation of the biexciton ground state has been obtained by two-photon absorption,[14–17]

$$E_{\rm Bi}(K)=E_{\rm Bi}+\frac{\hbar^2K^2}{2m_{\rm Bi}}, \tag{14}$$

where $E_{\rm Bi}$ is the biexciton energy and $m_{\rm Bi}$ its total mass,

$$E_{\rm Bi}=6.372\text{ eV}, m_{\rm Bi}=2m_{\rm ex}.$$

An important feature of the lower transverse polariton branch is the so-called polariton bottleneck. It is located around E_T and corresponds to the region of maximum density of states and minimum group velocity.[31]

The transmission-spectroscopy experiments reported here allow us to probe the time evolution of excitonic populations in different excited states. The optical density $\mathcal{H}$ induced in the crystal at a photon energy ω at a time delay τ between the test and the pump pulses is given by

$$\mathcal{H}(\hbar\omega,\tau)=-\log_{10}\left[\frac{I_t(\hbar\omega,\tau)}{I_t(\hbar\omega,\tau=-\infty)}\right], \tag{15}$$

where I_t is the transmitted test-beam intensity. Figure 4

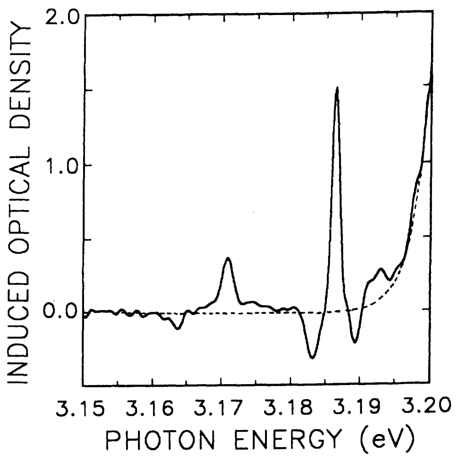

FIG. 4. Solid line is the induced optical density at zero time delay between pump and test pulses for $I_p=15$ MW cm^{-2}. Dotted line is the exponential fit to the induced absorption tail near the exciton resonance as described by Eq. (16) of the text.

shows a typical spectrum obtained at $\tau=0$ with a pump power of 15 MW cm^{-2}. When the test photon energy approaches E_T, a strong value of $\mathcal{K}$ is measured. It corresponds to a collision-induced broadening of the one-photon exciton absorption resonance.[32,33] It has been previously reported that the spectral shape of this absorption band follows closely an exponential dependence on photon energy. It can therefore be numerically removed from the data using

$$\mathcal{K}(\hbar\omega,\tau)=\mathcal{K}_0+\mathcal{K}_1\exp[-(\hbar\omega-E_0)/\gamma] \ . \tag{16}$$

The time evolution of the remaining induced optical density $\mathcal{K}$ is shown in Figs. 5(a)–5(d) for increasing pump-power densities. Figure 6 shows details of Fig. 5(c) for two time delays (0 and 50 ps), together with a luminescence spectrum measured under the same excitation conditions, with the iris diaphragm at the entrance of the spectrometer fully opened.

The different structures observed can be associated with three different types of process: (i) $\hbar\omega=\hbar\omega_p$ is the resonant two-photon absorption (TPA) which creates biexcitons, (ii) $\hbar\omega>3.172$ eV is the coherent scattering processes involving photonlike polaritons, and (iii) $\hbar\omega<3.172$ eV is the induced absorption or gain due to excitonic and biexcitonic quasiparticles.

A. Two-photon absorption

The main absorption band, noted TPA in Fig. 5, is centered at $\hbar\omega=\hbar\omega_p$. It corresponds to the resonant absorption of one pump and one test photon. Its temporal half width is 50 ps, in agreement with what is expected from the convolution of two Gaussian pump pulses of 30 ps duration each. The time-integrated intensity of the TPA band varies slightly sublinearly with the intensity of the pump beam, indicating saturation effects.

The average density of biexcitons n_{Bi} created by the simultaneous absorption of two photons of the pump beam can be approximately determined from the observed variation of the optical density induced at $\hbar\omega=\hbar\omega_p$ by the pump beam. The corresponding values are given in Table I.

B. Coherent scattering processes

While biexcitons keep their coherence properties of creation through the pump pulse, a strong parametric emission takes place. At small angles of incidence, it is expected to occur at spectral positions $\hbar\omega_{R_T^\pm}$ which are given by

$$2\hbar\omega_p-\hbar\omega_{R_T^\pm}=\hbar\omega_{R_T^\mp} \ . \tag{17}$$

R_T^+ and R_T^- represent the hyper-Raman emission lines that have been observed at the spectral positions given by (17), respectively, on the high- and low-energy sides of the laser pump. It corresponds to a nondegenerate four-wave mixing of the pump and of the test beams. For a given time delay between the test and pump pulses, this signal is maximum when the phase-matching conditions are fulfilled and when the test pulse induces the recombination of the biexcitons which have kept their wave vector of creation. This induced process corresponds to the well-known hyper-Raman scattering, in which the spontaneous recombination of these biexcitons occurs, the phase matching being automatically realized.

Table II gives the photon energies of these parametric

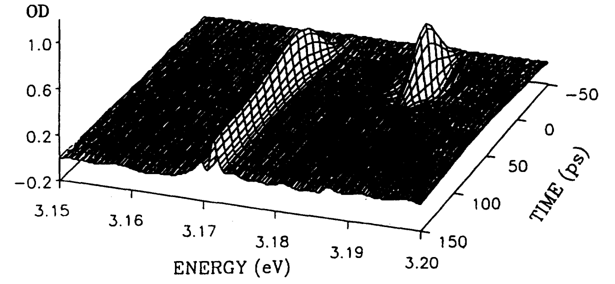

(a) E_p= 3.186 eV
I_p= 1.5 MW/cm^2

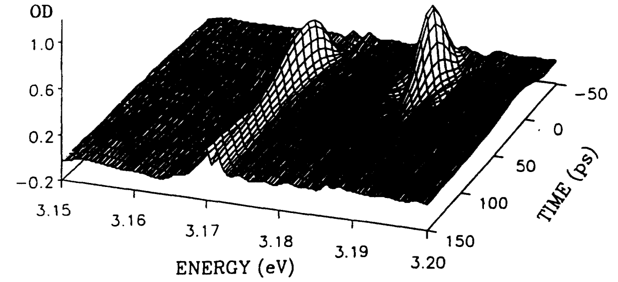

(b) E_p= 3.186 eV
I_p= 5 MW/cm^2

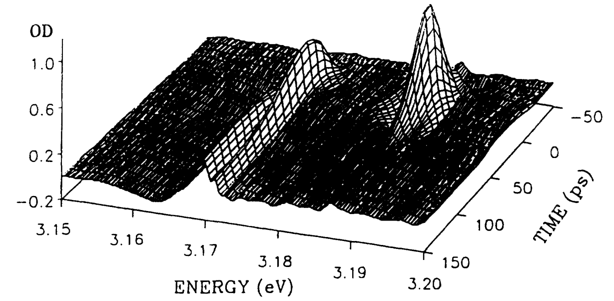

(c) E_p= 3.186 eV
I_p= 15 MW/cm^2

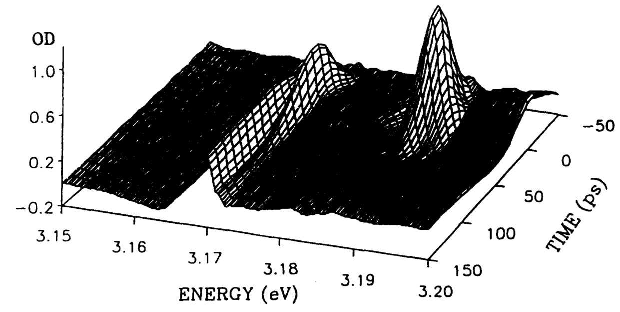

(d) E_p= 3.186 eV
I_p= 50 MW/cm^2

FIG. 5. Induced optical density as a function of time and photon energy for pump intensities of (a) 1.5, (b) 5, (c) 15, and (d) 50 MW cm^{-2}.

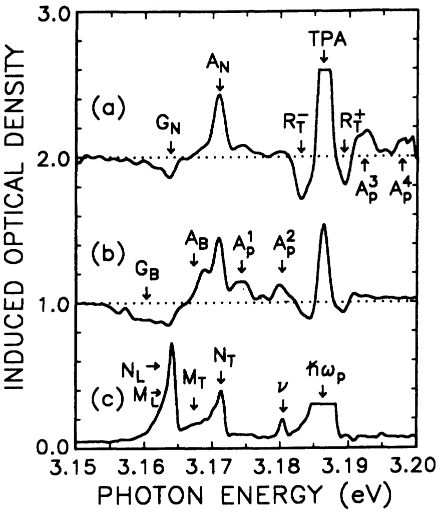

FIG. 6. Induced optical density for $I_p = 15$ MW cm^{-2} and a time delay between pump and test pulses of (a) 0 and (b) 50 ps. (c) shows the integrated luminescence of the sample under the same experimental conditions.

emission bands at the temporal coincidence of pump and test pulses, as obtained from Fig. 6(a). As can be seen in Fig. 6(b), the photon energies of these bands vary in time. This is the signature of the temporal change of the polariton dispersion when the exciton and the biexciton densities vary.

Four weak absorption bands, labeled A_p, are also observed in the same spectral region. We could attribute them to scattering processes of higher orders, induced by the pump pulse. They will be further discussed in Sec. V.

C. Induced absorption and gain

The resonantly created biexcitons rapidly lose their coherence with the pump beam through elastic and inelastic scattering. This happens in a time of the order of 50 ps, as can be seen when we compare the R_T line intensities in Figs. 6(a) and 6(b). However, since the absorbed photons have small wave vectors, the biexcitons are created at the bottom of their dispersion curve. They are called "cold" biexcitons because their kinetic energy is less than the thermal energy $k_B T$ of the lattice.

Due to wave-vector conservation, these cold biexcitons spontaneously decay either into small wave-vector longitudinal excitons called χ_L^0 and photonlike polaritons with a photon energy of $\hbar\omega = E_{\text{Bi}} - E_L$, or into transverse excitons located inside the bottleneck region (and labeled χ_T^0) and photonlike polaritons with a photon energy close to $\hbar\omega = E_{\text{Bi}} - E_T$. The photonlike polaritons transform into photons at the crystal surface and give rise to the emission lines N_L and N_T, observed in the time-integrated luminescence spectrum of Fig. 6(c).

TABLE I. Average density of biexcitons n_{Bi} as a function of the maximum of the pump-pulse intensity I_p.

I_p (Mw/cm^2)	n_{Bi}(10^{16} cm^{-3})
1.5	0.9
5	3
15	10
50	40

TABLE II. Photon energies of hyper-Raman scattering emissions as given in Ref. 28 and of the test-induced parametric emissions, as obtained from this work [Fig. 6(a)].

R_T^-	3.183 eV[a]	3.1828±0.0003[b]
R_T^+	3.189 eV[a]	3.1892±0.0002[b]

[a]From Ref. 28.
[b]This work [Fig. 6(a)].

As shown in Fig. 6(a), a narrow absorption band A_N develops rapidly at the spectral position of the N_T luminescence line. The induced absorption corresponds to the inverse process of the cold biexciton decay quoted above:

$$\hbar\omega_{\chi_T^0} + \hbar\omega_{A_N} = E_{\text{Bi}} \ . \tag{18}$$

The maximum of the A_N band is located at 3.171 eV.

A narrow gain band, labeled G_N, observed in Figs. 6(a) and 6(b), is also seen for small time delays between pump and test pulses at the spectral position of the N_L emission line. It corresponds to an induced recombination of cold biexcitons, which occurs at the following photon energy of the test:

$$\hbar\omega_{\chi_L^0} + \hbar\omega_{G_N} = E_{\text{Bi}} \ . \tag{19}$$

This band indicates that a population inversion exists between cold biexcitons and longitudinal excitons. Indeed, while the biexcitons are created in great numbers during the pump pulse excitation, the longitudinal excitons generated through the biexciton recombination thermalize and scatter rapidly to the lower polariton branch. Therefore, a population inversion takes place during the pump excitation.

The fact that an absorption line A_N, rather than a gain band, is observed for the transitions between cold biexcitons and polaritons indicates that the biexciton lifetime is short enough so that no inversion between biexcitons and excitonic polaritons can be achieved, even during the pump excitation.

Biexcitons can also be created by inelastic collision between excitons. The cross section of this process is quite large since the biexciton excess energy, equal to $2E_x - E_{\text{Bi}}$ ($\simeq 30$ meV), can be removed by an LO phonon emission (25 meV) followed by an acoustic phonon emission.[7] This process gives rise to a population of biexcitons with a high distribution of kinetic energy. These biexcitons with large wave vectors are called "hot" biexcitons in the following. They recombine into transverse or longitudinal excitons χ_T^* and χ_L^*, which also have large wave vectors, and photonlike polaritons with energies several meV below the observed N_L and N_T luminescence lines. These processes give rise to the M_L and M_T luminescence bands observed in the luminescence spectrum of Fig. 6(c).

As for cold excitons, the hot excitons (i.e., with large wave vectors) created by the decay of hot biexcitons also show up in absorption. In Fig. 6(b), the broad absorption band A_B develops in time on the small-photon-energy side of the A_N band.

Hot biexcitons manifest themselves by a gain band G_B. It is spectrally broad compared to the G_N line. Hot biexcitons follow a Boltzmann distribution characterized by a temperature of about 50 K, which decreases with time. While this gain band is barely noticeable for the smallest pump power, its integrated intensity becomes comparable to the A_B absorption band for higher pump intensities.

Finally, we must notice that a line called v_2, attributed to the radiative decay of bound excitons, shows up in the luminescence spectrum of Fig. 6(c). However, no corresponding absorption line is observed in the induced absorption spectra of Figs. 6(a) and 6(b).

V. DISCUSSION OF THE EXPERIMENTAL RESULTS

A. R_T^-, R_T^+ and A_p bands

The gain bands located at $\hbar\omega_p-\Delta$ and $\hbar\omega_p+\Delta$, with $\Delta=3$ meV, are of similar origin to the R_T^- and R_T^+ hyper-Raman lines seen in emission spectroscopy. They appear through coherent processes governed by

$$\chi_{\rm NL}^{ts(-2,0)*}\delta(2\omega_p-\omega_t-\omega_s)\delta(2\mathbf{k}_p-\mathbf{k}_t-\mathbf{k}_s)\ .$$

They thus correspond to a two-photon absorption of the pump beam which creates coherent biexcitons, whose recombination is induced under energy and momentum conservation by the test beam, giving rise to a signal emission. The field of the signal beam shows up as a source term in Eq. (9).

The A_p^1, A_p^2, A_p^3, and A_p^4 absorption bands are, respectively, located at $\hbar\omega_p-4\Delta$, $\hbar\omega_p-2\Delta$, $\hbar\omega_p+2\Delta$, and $\hbar\omega_p+4\Delta$, with $\Delta=3$ meV. This appears to indicate that these bands arise through an enhancement of the coherent part of $\chi_{\rm NL}^{tt(0,0)}$ induced by the presence of both signal beams R_T^- and R_T^+ interacting with coherent biexcitons created by the pump beam.

We propose the following detailed model to explain the origin of the A_p absorption bands.

First, R_T^+ and R_T^- photons are created with equal densities and similar temporal dynamics by the nonlinear interaction between pump and test pulses, verifying the equation of energy conservation

$$\hbar\omega_{R_T^+}+\hbar\omega_{R_T^-}=2\hbar\omega_p \tag{20}$$

and the phase-matching conditions.

Then, two $R_T^+(R_T^-)$ photons can form a real (virtual) biexciton with an energy above (below) the energy of the biexciton ground state at $\mathbf{K}=0$. These processes are schematically represented in Fig. 7(a). While the recombination of a virtually created biexciton is immediately induced by a pump photon, a really created biexciton remains in its state of creation during its coherence time. Its recombination can then be induced by a pump photon. Both processes again fulfill phase-matching conditions and energy conservation relations

$$2\hbar\omega_{R_T^{+,-}}-\hbar\omega_p=\hbar\omega_{s^{2,3}}\ , \tag{21}$$

where $s^{2,3}$ denote the photons generated throughout the two processes. They show a different temporal behavior. They propagate in the crystal with slightly different group velocities and are reabsorbed with photons of the test beam, giving rise to the A_p^2 and A_p^3 absorption bands,

$$\hbar\omega_{s^{2,3}}+\hbar\omega_{A_p^{2,3}}\simeq E_{\rm Bi}\ . \tag{22}$$

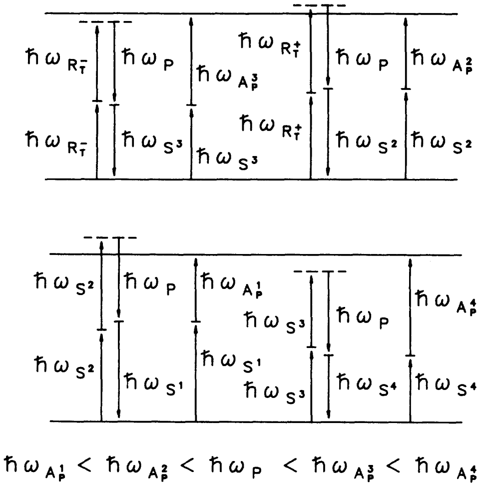

FIG. 7. Schematical representation of the different processes, giving rise to the A_p^1 to A_p^4 absorption lines.

The time dependence of these absorption bands is given in Fig. 8. The time delay (40 ps) between the maximum of the A_p^2 band (the dotted line) and the two-photon absorption band (the solid line) is due to the lifetime of the coherently created biexcitons which introduces a delay between the absorption and the induced recombination. This value is in agreement with the biexciton coherence time obtained from four-wave-mixing experiments[34,35] (10–40 ps depending on the excitation conditions[34]). The slight asymmetry of the temporal evolution of the A_p^3 band, which has its maximum before the maximum of the TPA may be due to an increase of the absorption during the excitation.

The thus-created S^2 and S^3 photons can follow the same cycle of absorption and recombination with test and pump photons. They give first rise to new parametric signals labeled S^1 and S^4. They obey

$$2\hbar\omega_{s^{2,3}}-\hbar\omega_p=\hbar\omega_{s^{1,4}}\ , \tag{23}$$

and to absorption bands A_p^1 and A_p^4 verifying the relation

$$\hbar\omega_{s^{4,1}}+\hbar\omega_{A_p^{4,1}}\simeq E_{\rm Bi}\ . \tag{24}$$

In Table III, the observed spectral positions of the different A_p bands are compared to the ones calculated for the previously described processes. The intensity of excitation is 15 MW/cm^2.

These processes are highly resonant on exciton and biexciton states. They thus require a high density of coherent "cold" biexcitons to be observed. This explains

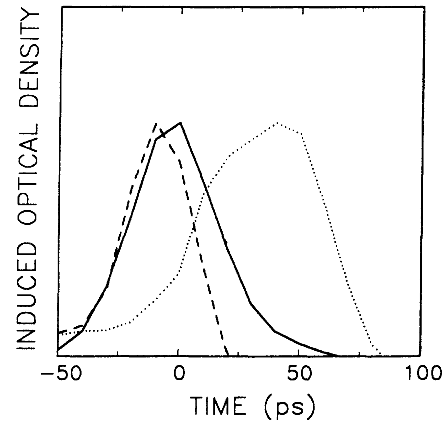

FIG. 8. Temporal evolution of the TPA (solid line), the A_p^2 band (dotted line), and the A_p^3 band (dashed line) for $I_p = 15$ MW cm^{-2}.

why such a hierarchy of coherent processes has not been previously reported.

B. A_N and G_N bands

The density of states on the biexciton level is higher than the density of states on the longitudinal exciton level by the ratio m_{Bi}/m_L. Moreover, longitudinal excitons rapidly scatter down to lower-lying transverse polariton states. A population inversion therefore builds up between the cold biexcitons and the χ_L^0 population. Probe-stimulated decay of biexcitons towards small wave-vector longitudinal exciton states is therefore favored, resulting in the G_N band.

As explained previously, the A_N absorption line corresponds to the reabsorption of cold excitonlike polaritons towards biexciton states. These polaritons have their origin in the radiative recombination of the initially created cold biexcitons. Therefore we analyze the temporal evolution of the A_N band by the convolution of the TPA absorption (A_{TPA}) by a sum of two exponential decay expressions,

$$A_N(t) \propto \int_0^t A_{\mathrm{TPA}}(t-t')(e^{-t'/\tau_1} + ce^{-t'/\tau_2})dt' \; . \tag{25}$$

The first one corresponds to a population of cold excitons created by the test-induced decay of biexcitons. They are generated at a high density and therefore couple efficiently to form hot biexcitons. In this case, the characteristic time constant which appears in the time integral is the lifetime τ_1 of cold biexcitons and not that of the excitons.

TABLE III. Spectral positions of the A_p bands (experimental and calculated values).

		Calculated positions	Experimental values
A_p^1	$E_{\mathrm{Bi}} - 5\hbar\omega_p + 4\hbar\omega_{R_T^-}$	3.1732±0.0008	3.1734±0.0004
A_p^2	$E_{\mathrm{Bi}} - 3\hbar\omega_p + 2\hbar\omega_{R_T^-}$	3.1796±0.0004	3.1798±0.0004
A_p^3	$E_{\mathrm{Bi}} - 3\hbar\omega_p + 2\hbar\omega_{R_T^+}$	3.1924±0.0004	3.1918±0.0004
A_p^4	$E_{\mathrm{Bi}} - 5\hbar\omega_p + 4\hbar\omega_{R_T^+}$	3.1988±0.0008	3.1979±0.0004

The second one corresponds to the decay of the remaining cold exciton population once a low density regime is reached. τ_2 represents the real lifetime of this population.

The experimental values of the integrated A_N bands are plotted in Fig. 9 as functions of test-pump delays and compared to the temporal evolution calculated from the preceding equation.

When we take into account only one exponential decay represented by τ_1, we obtain the solid lines in Fig. 9. We reproduce quite well the experimental data during the pump excitation but poorly at longer delays. The values of τ_1 obtained are given in Table IV. They diminish when the pump-excitation intensity increases. This variation of τ_1 is due to the intensity dependence of the biexciton decay times which shorten at higher pump intensities due to collisions.[34] In addition, when the density of cold polaritons increases, more hot biexcitons are formed. Therefore, at higher pump-power density, the A_N absorption is quenched and replaced by the A_B absorption band as we will discuss later on.

Concerning the second exponential contribution, characterized by the time constant τ_2, we obtain the calculated curves drawn as dotted lines in Fig. 9. For instance, in Fig. 9(a), the dotted curve fits quite well the experimental points corresponding to a pump density of 1.5 MW/cm^2 with a value of $\tau_2 = 270$ ps. In Table IV are given the values of τ_2 for the different pump-power densities. τ_2 is significant for the lifetime of the cold exciton population which itself is density-dependent due to the mutual coupling of excitons. This identification of τ_1 and τ_2 is consistent with Ref. 36.

C. A_B and G_B bands

By the coupling of two cold excitonic polaritons, biexcitons are created with an excess energy of 30 meV.

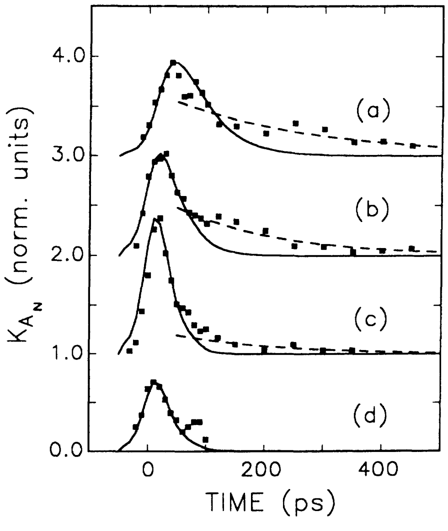

FIG. 9. Temporal evolution of the A_N absorption band for pump intensities of (a) 1.5, (b) 5, (c) 15, and (d) 50 MW cm^{-2}. ■, experimental data; solid line, short-time fit using Eq. (25) and the parameters of Table (IV); dashed line, long-time fit using the parameters of Table (IV).

TABLE IV. Time constants τ_1 and τ_2 characterizing the induced absorption A_N for cold exciton and biexciton populations.

I_p (MW/cm^2)	τ_1 (ps)	τ_2 (ps)
1.5	70	270
5	30	270
15	25	140
50	13	80

After emission of LO phonons, hot biexcitons with a high kinetic energy remain. Since radiative decay is their main recombination channel, their temporal evolution should be ruled by that of cold biexcitons. In the gain G_B observed here, they recombine, leaving longitudinal excitons with high kinetic energy which, as in the G_N process, scatter to the lower excitonic-polariton branch. Thus, the population inversion between biexcitons and longitudinal excitons is maintained.

To perform a quantitative analysis of the G_B band, we integrate the rate equation

$$\frac{dN_{\mathrm{Bi}}}{dt}=G-\frac{N_{\mathrm{Bi}}}{\tau_3}\ , \qquad (26)$$

where the generation rate G is assumed to be proportional to the number of cold excitons squared, which has been measured through A_N.

With this model, we fit the experimental points with the calculated curve given in solid line (Fig. 10). The time constants τ_3 for different intensities are given in Table V. In the frame of this model, τ_3 is not the lifetime of the biexcitons which is itself quite small ($\lesssim 30$ ps, see Table IVa), but simply reflects the lifetime of hot excitons. The discrepancies between the experimental data and the solid curve are probably due to the difficulty to discriminate G_B from the induced absorption A_B with sufficient precision.

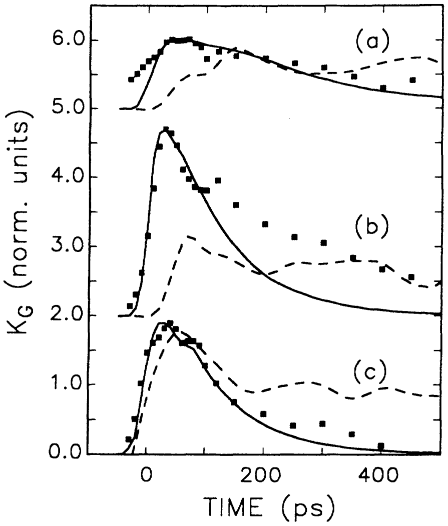

FIG. 10. Temporal evolution of the G_B gain bands for pump intensities of (a) 5, (b) 15, and (c) 50 MW cm^{-2}. ■, experimental data; solid line, fit to the data using Eq. (26) of the text and the parameters of Table (V); dashed line, temporal evolution of the A_B absorption band.

TABLE V. Time constants τ_3 characterizing the gain for hot exciton and biexciton populations.

I_p (MW/cm^2)	τ_B (ps)
5	180
15	95
50	95

A_B, drawn as dotted lines in Fig. 10, is spectrally situated between A_N and G_N. It is therefore perturbed by these two processes. Nevertheless, if one makes an analysis of its time variation in the same way as we did for A_N, one finds the same order of magnitude for its time constant ($\simeq 200$ ps).

Also, despite the difficulty explained above, an interesting feature to notice is the delay between the rising times of the A_B and the G_B bands. It confirms our previous statement that the biexciton lifetime is quite short, since it is given by the delay between gain and absorption. Again, we find a decrease of this delay from 50 to 10 ps when we change the pump-pulse intensities from 5 to 50 MW/cm^2.

VI. CONCLUSION

We have studied in this publication the relaxation and recombination processes of excitons and biexcitons in CuCl at low temperature. As shown in Fig. 3, an initial population of "cold" biexcitons[2] of small kinetic energy is first created by "resonant two-photon absorption"[1] of 30-ps laser pulses. These biexcitons relax and recombine, giving rise to "cold" longitudinal exciton and excitonic polaritons[3] with small kinetic energy. Due to a population inversion, the biexciton decay into longitudinal excitons can be stimulated or induced by 30-ps-long, spectrally broad test pulses of small intensity. This process shows up as gain in the transmission spectrum of time-delayed test pulses. Thus the lifetime of the cold biexciton population could be obtained. The temporal characteristics of cold excitonic polaritons, on the contrary, could be determined from the induced absorption due to the inverse process. In addition, in this same time range, several resonant parametric processes could be identified.

Furthermore, cold excitonic polaritons created from the initial biexciton recombination process can couple and generate "hot" biexcitons[4] with a high kinetic energy. Their dynamics shows up in a gain process in which "hot" longitudinal excitons[5] with high kinetic energy are generated. They can also thermalize into "hot" transverse excitons[5] with high kinetic energy. Their temporal characteristics are obtained once again by induced-absorption study. These secondary processes start about 50 ps after the excitation. They last as long as a high density of excitations is present inside the sample.

In addition to the measurement of the excitonic polariton lifetime, we obtain the important result that these complex dynamics can be fully understood if we assume that biexcitons (cold and hot) have short lifetimes (between 10–50 ps depending on the density of initially created biexcitons). These values are equal to the coherence times of biexcitons as determined in luminescence or two-beam transient-grating experiments for different excitation intensities. This numerical agreement between the two characteristic time constants of the biexcitons as well as their similar dependence on the excitation intensity clearly indicates that biexcitons do not relax or thermalize through scattering processes but essentially recombine through radiative processes. The thermalization of the exciton-biexciton population is achieved through collisions inside the exciton population.

ACKNOWLEDGMENTS

The authors are grateful to Professor H. Haug for many helpful discussions when he was at the University Louis Pasteur of Strasbourg and to Professor R. Lévy for many helpful discussions. The numerical calculations have been performed at the "Centre de Calcul du CNRS." The Institut de Physique et Chimie des Materiaux de Strasbourg is "Unité mixte" of the University Louis Pasteur, the Ecole Européennes des Hautes Etudes des Industries Chimiques and the Centre National de la Recherche Scientifique No. 380046.

---

*Permanent address: Département de Physique, Université de Montréal, CP 6128, Succ. "A," Montréal, Québec, Canada H3C 3J7.

†Present address: Département de Physique, Faculté des Sciences d'Agadir, Université Ibnou Zohr, Agadir, Morocco.

[1] J. J. Hopfield, Phys. Rev. **112**, 1555 (1958).

[2] S. I. Pekar, Zh. Eksp. Teor. Fiz. **33**, 1022 (1958) [Sov. Phys. JETP Lett. **6**, 785 (1958)].

[3] V. M. Agranovich, Zh. Eksp. Teor. Fiz. **37**, 430 (1960) [Sov. Phys. JETP Lett. **10**, 307 (1960)].

[4] B. Hönerlage, R. Levy, J. B. Grun, C. Klingshirn, and K. Bohnert, Phys. Rep. **124**, 161 (1985).

[5] R. Levy, B. Hönerlage, and J. B. Grun, Helv. Phys. Acta **58**, 252 (1985).

[6] J. B. Grun, B. Hönerlage, and R. Levy, in *Excitons,* Vol. 2 of *Modern Problems in Solid State Physics,* edited by E. I. Rashba and M. D. Sturge (North-Holland, Amsterdam, 1982), p. 459.

[7] R. Levy, B. Hönerlage, and J. B. Grun, in *Optical Nonlinearities and Instabilities in Semiconductors,* edited by H. Haug (Academic, New York, 1988), p. 181.

[8] Vu Duy Phach, A. Bivas, B. Hönerlage, and J. B. Grun, Phys. Status Solidi B **86**, 159 (1978).

[9] T. Itoh, T. Suzuki, and M. Ueta, J. Phys. Soc. Jpn. **42**, 1069 (1977).

[10] B. Hönerlage, A. Bivas, and Vu Duy Phach, Phys. Rev. Lett. **41**, 49 (1978).

[11] T. Mita, K. Satomé, and M. Ueta, Solid State Commun. **33**, 1135 (1980).

[12] D. Fröhlich, E. Mohler, and P. Wiesner, Phys. Rev. Lett. **26**, 554 (1971).

[13] J. K. Pribam, G. L. Koos, F. Bassani, and J. P. Wolfe, Phys. Rev. B **28**, 1048 (1983).

[14] E. Hanamura, Solid State Commun. **12**, 951 (1973).

[15] Vu Duy Phach, A. Bivas, B. Hönerlage, and J. B. Grun, Phys. Status Solidi B **84**, 731 (1977).

[16] R. Levy, B. Hönerlage, and J. B. Grun, Phys. Rev. Lett. **44**, 1355 (1981).

[17] T. Mita, K. Satomé, and M. Ueta, J. Phys. Soc. Jpn. **48**, 496 (1980).

[18] R. Levy, B. Hönerlage, and J. B. Grun, Phys. Rev. B **19**, 2326 (1979).

[19] Y. Masumoto and S. Shionoya, J. Phys. Soc. Jpn. **51**, 151 (1981).

[20] H. Haug, in *Festkörperprobleme XX,* edited by J. Treusch (Vieweg, Braunschweig, 1982), p. 149, and references cited therein.

[21] V. May, K. Henneberger, and F. Henneberger, Phys. Status Solidi B **94**, 611 (1979).

[22] J. Y. Bigot and B. Hönerlage, Phys. Status Solidi B **121**, 649 (1984).

[23] B. Hönerlage and J. Y. Bigot, Phys. Status Solidi B **123**, 201 (1984).

[24] B. Hönerlage and J. Y. Bigot, Phys. Status Solidi B **124**, 221 (1984).

[25] J. B. Grun, B. Hönerlage, and R. Levy, Solid State Commun. **46**, 51 (1983).

[26] B. Hönerlage, R. Levy, and J. B. Grun, Opt. Commun. **43**, 443 (1982).

[27] B. Hönerlage, J. Y. Bigot, F. Tomasini, and J. B. Grun, Solid State Commun. **48**, 803 (1983).

[28] R. Levy, J. Y. Bigot, B. Hönerlage, F. Tomasini, and J. B. Grun, Solid State Commun. **48**, 705 (1983).

[29] R. Levy, B. Hönerlage, and J. B. Grun, Philos. Trans. R. Soc. London Ser. A **313**, 229 (1984).

[30] S. S. Montasser, J. Miletic, and B. Hönerlage, Phys. Rev. B **40**, 6163 (1989).

[31] B. Hönerlage, R. Levy, and J. B. Grun, in *Progress on Electron Properties of Solids,* edited by R. Girlanda *et al.* (Kluwer Academic, Amsterdam, 1989), p. 275.

[32] R. Leonelli, J. Ch. Mathae, J. M. Hvam, F. Tomasini, and J. B. Grun, Phys. Rev. Lett. **58**, 1363 (1987).

[33] H. Haug, J. Liebler, R. Leonelli, A. Manar, and J. B. Grun, Phys. Rev. B **38**, 10 903 (1988).

[34] R. Levy, M. J. Matos Gomes, B. Kippelen, and B. Hönerlage, Phys. Status Solidi B **158**, 391 (1990).

[35] M. J. Matos Gomes, R. Levy, and B. Hönerlage, J. Lumin. **48/49**, 83 (1991).

[36] H. Akiyama, K. Kuwata, T. Kuga, and M. Matsuoka, Phys. Rev. B **39**, 12 973 (1989).

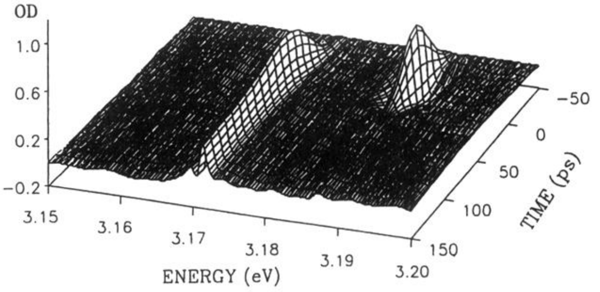

(a) $E_p = 3.186$ eV
$I_p = 1.5$ MW/cm^2

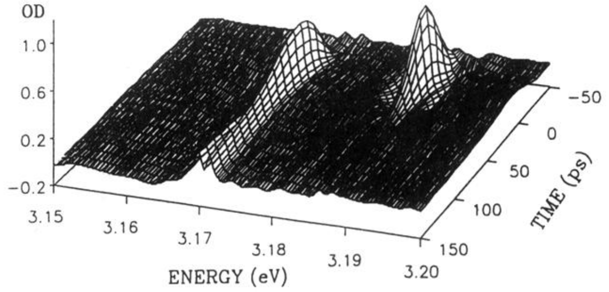

(b) $E_p = 3.186$ eV
$I_p = 5$ MW/cm^2

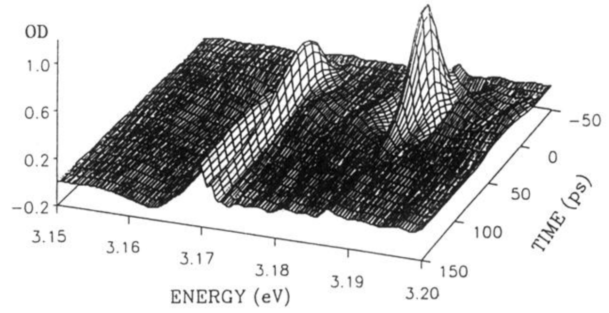

(c) $E_p = 3.186$ eV
$I_p = 15$ MW/cm^2

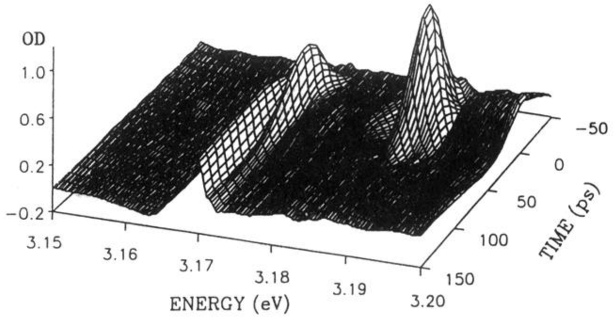

(d) $E_p = 3.186$ eV
$I_p = 50$ MW/cm^2

FIG. 5. Induced optical density as a function of time and photon energy for pump intensities of (a) 1.5, (b) 5, (c) 15, and (d) 50 MW cm^{-2}.